

# Large Eddy Simulation of Distillation Sieve Tray Hydrodynamics using Volume-of-Fluid (VOF) Multiphase Model

A. Malvin, A. Chan, and P. L. Lau

**Abstract**—A computational fluid dynamics (CFD) model is developed to predict the hydrodynamics and hydraulics of industrial-scale distillation sieve tray. Three-dimensional two-phase flow of gas and liquid is considered in which the interaction was modeled based on the concept of phasic volume defined in the Volume of Fluid (VOF) multiphase model through Large Eddy Simulation (LES). All governing equations including surface tension and wall adhesion are solved simultaneously using the FLUENT code. This preliminary work focuses on the improvement of the existing Reynolds-Averaged Navier-Stokes (RANS) based models in term of accuracy relative to experimental data. The computational domain and operating conditions were adapted from experimental study [1] where liquid velocity profiles, clear liquid height, and flow patterns were among the important quantities monitored. Gas-liquid interfaces and the existence of froth regime are clearly visualized via VOF model. The predicted quantities are found out to be in very good agreement with experimental data having discrepancies of less than 1.0%. Mesh resolutions above the bubbling area is identified as the key factor in accurate modeling of sieve tray hydrodynamics. The present model can be utilized with high confidence as the basis for the optimization of sieve tray mechanical design.

**Index Terms**—Large Eddy Simulation (LES), sieve tray, Volume-of-Fluid (VOF).

## I. INTRODUCTION

For the past decades, numerous works had been done to improve the efficiency of separation process in a tray distillation column. The majority, if not all, of these works were conducted in experimental manner aiming to correlate physical quantities observed under varying operating parameters. However, as resources become more and more scarce and with the ever growing pressures from global communities to reduce carbon dioxide emissions, efficiency has again emerged as a prominent issue especially for this high energy demanding unit operation.

Major improvement in computer technology, advancements in numerical methods and progression in multiphase flow models have allowed the use of computational fluid dynamics (CFD) technique in the study of intrinsically complex flow problems in distillation trays. Appreciable amount of computational studies, coupled by

validation with reliable experimental data, have been conducted in the past ten years. Mehta *et al.* [2] simulated the liquid velocity distribution in an industrial-scale sieve tray by solving the liquid time-averaged equations of continuity of mass and momentum in a single phase steady-state three dimensional system. The presence of gas phase was, however, taken into account by introducing a liquid phase volume fraction term in the transport equation. The assumption of constant liquid volume fraction and the absence of vapor phase transport equation were identified as the main factors in the discrepancies from the experimental data. Yu *et al.* [3] developed a two-fluid two-dimensional flow model which introduces another set of transport equations to the dispersed vapor phase. This model rectified the deficiency found in the model proposed by [2]. Two-equation  $k-\varepsilon$  turbulence model was utilized as the equations closure model. The resultant observation showed a good agreement with those published by [4] for outlet weir height of 50 mm. Severe discrepancies were, however, observed in the case when outlet weir height is 20 mm. This is due to the fact that at the near-wall, viscous force contributes to the formation of three-dimensional flow where the variation of velocity along the vertical direction is significant. Hence the prediction of two-dimensional theoretical model is invalid. Computational study on the effect of liquid loading, superficial gas velocity and weir height to clear liquid height was first attempted by [5]. The clear liquid height is defined by the height to which the aerated mass would collapse in the absence of vapor flow [6]. Volume-averaged mass and momentum conservation equations were solved in an Eulerian framework applying  $k-\varepsilon$  turbulence model. A non-conventional rectangular tray and sieve holes were used in this simulation. Computational results obtained show a good agreement with correlation proposed by [7]. Deviations were, however, observed when compared to the experimental data and correlation by [8]. These discrepancies were contributed by inadequate modeling of turbulence phenomena and the use of non-conventional design of tray and sieve holes. The use of rectangular holes geometry would influence the results associated with the use of Volume of Fluid (VOF) simulations for a priori prediction of bubble dynamics. Using the same turbulence and multiphase model, Van Baten and Krishna [9] simulated the tray hydrodynamics in a small-scale circular tray. Although tray hydraulics was well modeled, no attempt was made to validate the fluid flow patterns of industrial-scale sieve tray. Detailed works

Manuscript received July 02, 2010.

A. Malvin, A. Chan and P. L. Lau are with the Division of Environment, Faculty of Engineering, University of Nottingham in Malaysia, Jalan Broga, 43500 Semenyih, Selangor Darul Ehsan, Malaysia (phone: 603-8924-8622; fax: 603-8924-8017; e-mail: kebx8amv@ nottingham.edu.my).

involving the use of two-fluid Eulerian-Eulerian framework were conducted by [10]. The extended downcomer region allows complete simulation of fluid flow behavior in this region. Apart from this, liquid flow nonidealities namely stagnant zone, liquid recirculation and channeling were successfully modeled. Slight discrepancies on clear liquid height were observed when comparing with correlation by Bennett *et al.* [7]. The results obtained tend to overpredict the clear liquid height. However, [9] and [10] agreed that these discrepancies were caused by the intrinsic limitation of the empirical correlations when dealing with froth regime.

The computational works conducted in the past decade share one similarity which is the use of  $k-\varepsilon$  turbulence model as closure to the equation sets. The underlying reason is the relatively less expensive computational cost. However, the  $k-\varepsilon$  turbulence model performs poorly in three dimensional flows and flows in the near wall region whereby the presence of shear is strong. Extensive works had been done by [11] to investigate the performances of different turbulence models mainly in the near-wall region. The results of the investigation concluded that no current Reynolds-averaged turbulence models (RANS) can predict the whole range of complex turbulent flows to worthwhile engineering accuracy. Although the Reynolds Stress Model (RSM) did appear to be superior to the Eddy Viscosity Model (EVM) and two-equation models, it is insufficient to warrant the abandonment of eddy-viscosity models.

The main objective of this work is to develop a computational model that rectifies most of the discrepancies found in the previous computational works by incorporating the Large Eddy Simulation (LES) turbulence model as closure to equations sets and employing the VOF multiphase model which enable clear visualization of gas-liquid interfaces at any point in the system. The computational domain is generated based on the 1.213 m in diameter industrial-scale sieve tray used in experimental works by [1] involving an air-water binary system. Validation works will be based on comparison between computational results and published experimental data.

## II. COMPUTATIONAL GEOMETRY

Three-dimensional geometry, identical to the experimental sieve tray used in [1], is developed using commercial software called GAMBIT. The computational domain models an industrial-scale sieve tray with diameter of 1.213 m. Detail specifications of the sieve tray geometry are presented in Table II. Only half tray is modeled following observation of symmetric flow about the tray centre by [1]. Such configuration results in relatively less computational cost and time. To allow full modeling of tray hydrodynamics, total numbers of 175 sieve holes are generated each with diameter of 12.7 mm, arranged in a 0.05 m triangular pitch as shown in Fig. 1. Downcomer region is included to allow better representation of actual flow behavior inside a tray column.

The computational domain consists of hexahedral and polyhedral meshing elements. Mesh gradients were employed to the system with the active region ( $0m < y < 0.038m$ ) and the flow transition region

( $0.038m < y < 0.3m$ ) having interval sizes of 0.0095 m and 0.018 m respectively, as shown in Fig. 2.

It is crucial to have sufficiently high mesh resolutions at these regions to attain accurate representation of gas-liquid interaction consequently the prevailing flow regime. Coarse meshes are applied to the remaining domain considering their minimum contributions to the system hydrodynamics. The number of computational cells generated ranges from 100,000 – 250,000 cells. Difficulty in meshing arises from the presence of sieve holes which prevent the generation of high quality structured hexahedral meshing elements.

**Table II.** Sieve tray specifications.

Description	Dimension (m)
Diameter, $d_T$	1.213
Hole diameter, $d_H$	0.0127
Weir height, $h_w$	0.05
Weir length, $L_w$	0.925
Tray Spacing, $S$	0.61
Clearance under downcomer, $h_{cl}$	0.038
% Bubbling area, $A_B$ (over total area)	76%

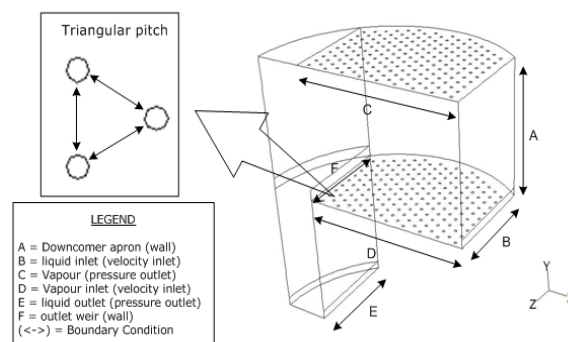


**Fig. 1.** Isometric view of computational geometry boundary conditions applied.

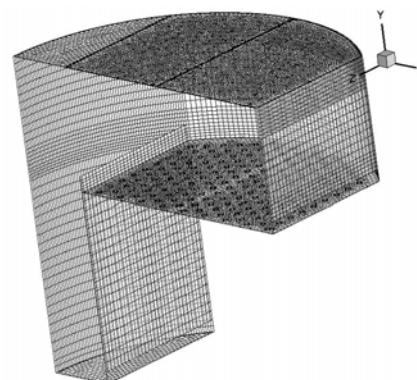


**Fig 2.** Mesh configurations of the computational domain.

### III. GOVERNING EQUATIONS

In the proposed VOF multiphase model the tracking of gas-liquid interfaces is accomplished by the solution of a continuity equation for the volume fraction ( $\alpha$ ) of the two phases. Since the main focus of this work is on the hydrodynamic behavior of sieve trays, mass and energy transfers are not considered. Hence for the  $q^{th}$  phase, the continuity equation has the following form:

$$\frac{\partial \alpha_q \rho_q}{\partial t} + (\nabla \cdot \alpha_q \rho_q u) = 0 \quad (1)$$

where  $u$  represents velocity. Having constant density ( $\rho$ ) and viscosity ( $\mu$ ), equation (1) reduces to

$$(\nabla \cdot \alpha_q u) = 0 \quad (2)$$

The volume fraction equation only solves for the secondary liquid phase whilst the primary gas phase volume fraction is computed based on the following constraint:

$$\sum_{q=1}^n \alpha_q = 1 \quad (3)$$

The momentum equation is given by:

$$\rho \left( \frac{\partial u_i}{\partial t} + u(\nabla \cdot u) \right) = -\nabla p + \mu \nabla^2 u + \rho g + F_{vol} \quad (4)$$

where  $p$  indicates pressure whilst  $g$  and  $F_{vol}$  represents gravitational acceleration and volume force respectively. Continuum surface force (CSF) [12] was used to model the surface tension which was taken into account via the source term,  $F_{vol}$ , in the momentum equation. For two-phase flow, the volume force is defined by:

$$F_{vol} = \sigma_{ij} \frac{\rho \kappa_i \nabla \alpha_i}{0.5(\rho_i + \rho_j)} \quad (5)$$

where subscript  $i$  and  $j$  denotes volume phases;  $\sigma$  represents the surface tension coefficient;  $\kappa$  represents the curvature defined by the divergence of the unit normal,  $\hat{n}$ :

$$\kappa = \nabla \cdot \hat{n} \quad (6)$$

where

$$\hat{n} = \frac{n}{|n|} \quad (7)$$

In which

$$n = \nabla \alpha_q \quad (8)$$

The significance of surface tension was determined by evaluating the Weber number,  $We$  which is given by:

$$We = \frac{\sigma}{\rho_L U^2} \quad (9)$$

where  $\rho_L$  represents liquid density;  $U$  represents the free-stream velocity and  $L$  represents the clearance under the downcomer.  $We \gg 1$  indicates that the presence of surface tension is significant and should not be neglected. In this work, given the air factor,  $F_s$  of 0.462, the calculated Weber number was approximately 7.3, indicating the strong influence of surface tension to the gas-liquid interface.

The governing equations employed for the Large Eddy Simulation (LES) are obtained by filtering the time-dependent Navier-Stokes equations in the physical space. In the CFD code, the filtering operation is implicitly provided by the finite-volume discretization. The filtered Navier-Stokes equations are:

$$\frac{\partial \alpha_q \bar{u}_i}{\partial x_i} = 0, \quad (10)$$

$$\rho \left( \frac{\partial \bar{u}_j}{\partial t} + \bar{u}_i \frac{\partial \bar{u}_j}{\partial x_i} \right) = -\frac{\partial \bar{p}}{\partial x_j} + \mu \frac{\partial^2 \bar{u}_j}{\partial x_i^2} - \frac{\partial \tau_{ij}^r}{\partial x_i} + \rho g + F_{vol} \quad (11)$$

where  $\bar{u}_i$  is the filtered resolved quantity in the  $i$ th direction;  $\bar{p}$  represents the filtered pressure, and  $\tau_{ij}^r$  is the residual stress tensor. Closure of the problems is achieved using the static Smagorinsky model [13]

$$\tau_{ij}^r = -2\nu_t \bar{S}_{ij} \quad (12)$$

where  $\bar{S}_{ij}$  represents the strain tensor given by:

$$\bar{S}_{ij} = \frac{1}{2} \left( \frac{\partial \bar{u}_i}{\partial x_j} + \frac{\partial \bar{u}_j}{\partial x_i} \right) \quad (13)$$

and  $\nu_t$  is the subgrid eddy viscosity given by:

$$\nu_t = l_s^2 S = (C_s \Delta)^2 S \quad (14)$$

where  $l_s$  is the Smagorinsky length scale;  $C_s$  is the Smagorinsky coefficient;  $\Delta$  is the subgrid scale characteristic length and  $S$  is the strain-rate tensor given by  $\sqrt{2}|S_{ij}|$ .  $C_s$  value of 0.1 was adopted since at this point the Smagorinsky's model behaves reasonably well for free-shear flows and for channel flow [14]. All of the above governing equations, (1) – (14), were solved simultaneously using the commercial code called FLUENT 6.3.

### IV. BOUNDARY CONDITIONS

#### A. Liquid Inlet

Proper boundary conditions have to be defined in order to solve the equations set uniquely. As shown in Fig. 1, instead of mass flow inlet, velocity-inlet was specified as the liquid inlet boundary condition. Experimentally, tray by tray measurement of liquid mass flow rate entering from downcomer clearance is difficult to conduct and accuracy is always an issue. Most of the time, it is more convenient to express this quantity in term of liquid volumetric flow rate,  $Q_L$ , given by:

$$u_{L,in} = \frac{Q_L}{A_{da}} \quad (15)$$

The area under the downcomer apron,  $A_{da}$  is given by the product of downcomer clearance height,  $h_{cl}$  and weir length,  $l_w$ . In present work, only liquid is assumed to enter the system ( $\alpha_L = 1$ ). This assumption is valid as the entrainment in this region is small and negligible [19]. In present work, only uniform flat liquid inlet profile was considered.

#### B. Gas Inlet

Similarly, velocity-inlet was specified as the gas inlet boundary condition. Direct measurement of gas velocity is often difficult to conduct experimentally, hence, a more convenient way is to express this quantity in term of superficial F-factor, often represented by  $F_S$ . This quantity is defined by the product of gas superficial velocity,  $V_S$  and square root of gas phase density,  $\rho_V$  as shown in the

following:

$$F_S = V_S \sqrt{\rho_V} \quad (16)$$

Taking  $V_S$  as subject, equation (16) is then rearranged to

$$V_S = \frac{F_S}{\sqrt{\rho_V}} \quad (17)$$

For any given vapor load, the vapor superficial velocity can hence be calculated via (17). Having the bubbling area  $A_B$  as the basis of superficial velocity, the gas inlet velocity is then given by:

$$u_{h,i} = \left( \frac{V_S A_B}{2N_H} \right) \frac{1}{A_{h,i}} \quad (18)$$

$N_H$  represents the number of sieve holes in the model geometry and  $A_{h,i}$  stands for the hole area. The inlet gas volume fraction was assumed to be unity. Although entrainment always exists in the real industrial operation, its contribution towards the hydrodynamics of sieve tray is not significant.

### C. Liquid and Gas Outlet

Pressure-outlet was specified as the liquid- and gas- outlet boundary conditions with backflow volume fraction of unity assigned at the secondary liquid-phase. This is to ensure that all of the downcoming liquid flows out via clearance under the downcomer apron. As such liquid and vapour flow across the tray are driven by the pressure gradient between the inlet and outlet of both entity.

### D. Geometry Wall and Plane Symmetry

No slip wall condition was specified to all wall boundaries. Wall adhesion was also modelled by specifying the contact angle between wall and liquid. Since no experimental values available in the literature, value of  $90^\circ$  was applied [15]. Planes indicating the centre of computational geometry were specified as symmetry boundary condition. At this plane, no flow and no scalar flux across the boundary occurs. Normal velocities are zero and the gradients of the other variables in the transverse coordinate direction are taken to be zero.

## V. OPERATING CONDITIONS AND SOLUTION ALGORITHMS

The simulations were carried out at slightly above the atmospheric condition (114,600 Pa) with reference pressure location at  $x=0$ ,  $y=0.5$  and  $z=-0.305$  [7]. Air and water are employed as the working fluids with air being specified as the primary gas phase whilst water being assigned as the secondary liquid phase. Since air is the dominant phase throughout the system, operating density was defined at  $1.225 \text{ kg/m}^3$  (density of the lightest phase, air).

The simulation is initialized by patching the liquid inlet surface with  $\alpha_L=1$  so that gas-liquid interfaces can be tracked immediately from the point of release. Apart from this, each time step was assumed to have fully converged whenever the continuity equation absolute criterion attained the value of 0.0001. This value is found to be adequate in assuring the convergence of the simulation based on the observation of liquid mass flow rate in the outlet stream and clear liquid height which are further discussed later. The most

important factor which affects the convergence of the simulation is the time-step size,  $\Delta t$ . In this work, the time-step size was evaluated based on the following relationship:

$$\Delta t = \frac{V_{cell,min}^{1/3}}{U} \quad (19)$$

where  $V_{cell,min}$  is the minimum volume of the computational domain whilst  $U$  represents the fluids inlet velocity. With different values of air and water inlet velocity, the time-step size calculated varies from 0.005 s to 0.0001 s. However, better convergence was observed at  $\Delta t=0.0001$  s.

Solution algorithms are introduced to enhance or accelerate the convergence of this simulation. The pressure velocity coupling was handled by the Semi-implicit Method for Pressure-linked Equation (SIMPLE) algorithm whilst Pressure Implicit with Splitting Operators (PRESTO) is used as the discretization method. The solution algorithms were chosen based on trial and error procedures with the mentioned combinations result in the fastest convergence in term of computational time, as shown in Table III. All of the simulations were conducted using 8 Intel Xeon processors 2.93 GHz run in parallels. Depending on the number of computational cells, computational time varies from 3 weeks to 6 weeks.

**Table III.** Performance of various pressure velocity coupling

Pressure velocity coupling	Wall-clock time per numerical iteration
SIMPLE	2 s
SIMPLEC	4 s
PISO	divergence

## VI. RESULTS ANALYSES AND DISCUSSIONS

### A. Convergence and Grid Independency Test

The transient simulation is deemed to have converged whenever the clear liquid height showed no considerable variation with time. At each time step, this variable is computed via the product of tray spacing and volume-average liquid phase volume fraction above the bubbling area of tray. As shown in Fig. 3, clear liquid height increased rapidly in the first 4s and gradually achieved steady-state after 8 s of computational flow-time. No significant variations are observed afterwards indicating the full convergence of computational flow-field. Sensitivity tests were therefore conducted by comparing the clear liquid height obtained from different grid sizes: 113,162 cells, 157,782 cells, 175,856 cells, 202,924 cells and 253,486 cells.

As shown in Fig. 4, clear liquid height varies significantly when grid sizes are less than 200,000 cells. Steady values are, however, observed at point beyond 200,000 cells. In spite of the precision offered at higher cell counts the use of

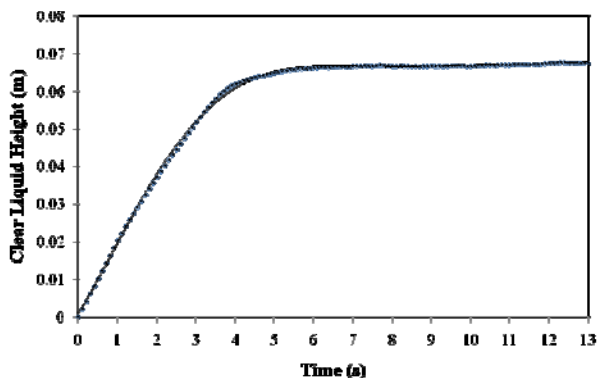


**Fig. 3.** Variation of clear liquid height as function of computational flow-time at  $Q_L = 17.8 \text{ m}^3/\text{s}$  and  $F_S = 0.462$ .

Ultra-fine meshes are avoided to reduce computational costs. Since any increment beyond this point sees no significant changes in clear liquid height, grid size of 202,924 cells is hereby chosen as base model for the analysis of tray hydrodynamics.

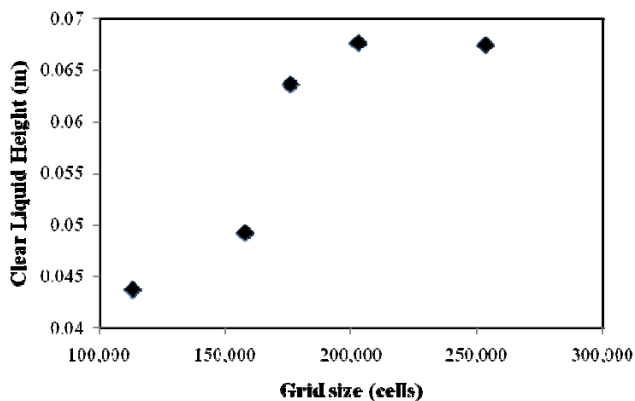


**Fig. 4.** Sensitivity of clear liquid height to grid resolutions.

### B. Clear Liquid Height

Validation of computational results is first carried out by comparing the calculated results with the published experimental data [1] and available correlations [7], [8]. As shown in Fig. 5, the proposed VOF-LES model shows remarkable accuracy, having maximum deviation of less than

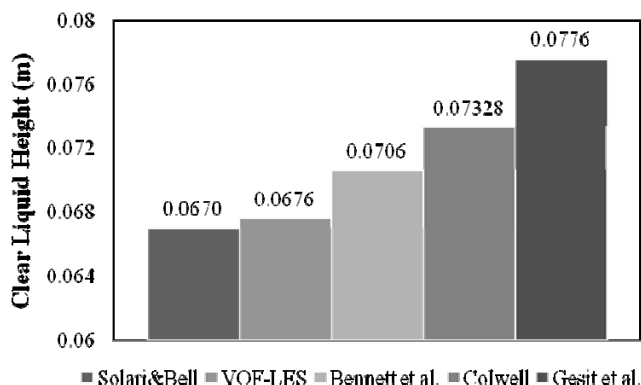


**Fig. 5.** Clear liquid height data at  $Q_L = 17.8 \text{ m}^3/\text{s}$  and  $F_S = 0.462$ .

1% from the experimental data. Meanwhile, Colwell and Bennett correlations deviate approximately 5.4% and 9.4% respectively whilst Eulerian-Eulerian- $k-\epsilon$  model proposed in [10] showing the largest discrepancy of 15.82%. The accuracy observed in VOF-LES model is due to the fact that

all large-scale anisotropy motions (geometry dependent) are computed explicitly while only the smaller scales motions (which have a universal character) are being modeled by the subgrid eddy viscosity model. As such, the use of LES in this case has enabled the observation of accuracy close to Direct Numerical Simulation (DNS) with significantly less computational costs. Meanwhile, Gesit *et al.* [10] pointed out that the discrepancies in the proposed Eulerian-Eulerian- $k-\epsilon$  model are contributed by the insufficient spatial resolution of the flow near the tray floor and the use of smaller number of sieve holes which leads to channeling, consequently an increased in clear liquid height. However, it has to be noted that the choice of turbulence model plays significant role in the accurate representation of flow phenomena prevailing inside the tray. Owing to the fact that the  $k-\epsilon$  turbulence model performs poorly in the system where the presence of shear is strong, it can hence be concluded that the choice of turbulence model is the main factor contributing to the major discrepancy in [10].

### C. Upstream and Downstream Liquid Velocity Profiles

Further validation work was carried out by comparison of liquid velocity profiles with the experimental data. As shown in Fig. 6, Solari & Bell [1] in their experimental study installed measuring probes at elevation of 0.038 m above the tray floor. These probes were used to obtain liquid velocity magnitude at corresponding points. Region bounded by  $x = -0.046$  and  $x = 0.183$  represents the upstream region whilst region bounded by  $x = -0.275$  and  $x = -0.046$  represents the downstream region. Liquid velocity magnitude was averaged along the x-axis as function of z-axis.

Unlike time-averaging method utilized in the RANS model, LES allows the evaluation of instantaneous velocity profiles across the tray. Velocity magnitude data can therefore be obtained at any point of time allowing close resemblance in terms of data sampling method used in the experimental work by [1]. Both upstream and downstream liquid velocity profiles are evaluated at computational flow-time = 13 s in which steady-state was observed, as shown in Fig. 3.

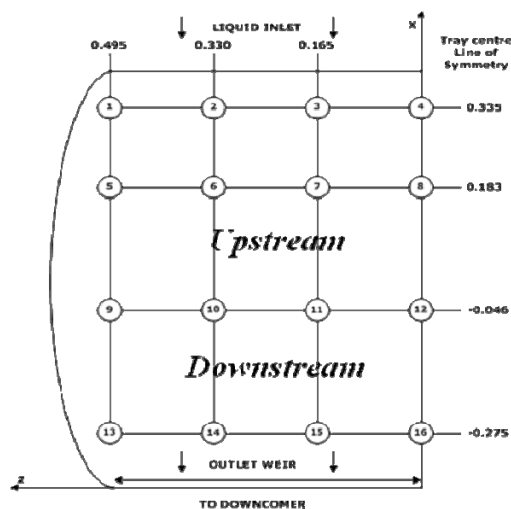


**Fig. 6.** Measuring probes position in the experimental work by Solari and Bell [1]. The diagram depicts half tray geometry in the absence of calming zone.

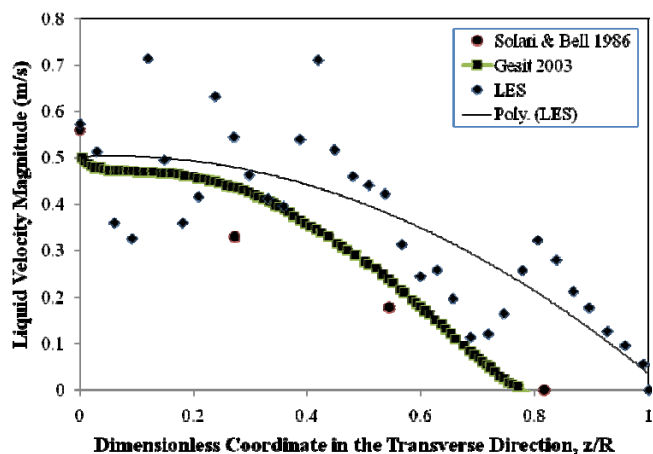


**Fig. 7.** Upstream liquid velocity profile at  $Q_L=17.8 \times 10^{-3} \text{ m}^3/\text{s}$  and  $F_S = 0.462$ .

It can be seen, from Fig. 7 and Fig. 8, that highest velocity magnitude exists in the region of tray centre. The magnitude then decreases gradually as it moves along the z-axis towards the column wall indicating the presence of non-uniform velocity distribution. Stagnant zone, represented by velocity magnitude of less than 0.1 m/s, can be clearly observed in the near-wall region ( $z/R \sim 1$ ). These observations are in good agreement with the experimental finding by [1]. Meanwhile, fluctuations in liquid velocity magnitudes are due to the contribution of upward gas phase momentum created by the injection of air via the sieve holes. In contrast to the Eulerian-Eulerian multiphase model, in VOF, fluids of different phases are not interpenetrating and that a single set of momentum equations is shared by the fluids. In other words, the velocity magnitude shown in Fig. 7 and Fig. 8 signify the mixture phase instead of individual liquid phase. In spite of the fluctuating parts, the overall trends correspond reasonably well with both [1] and [10], as shown by the Poly. (LES) trend line.

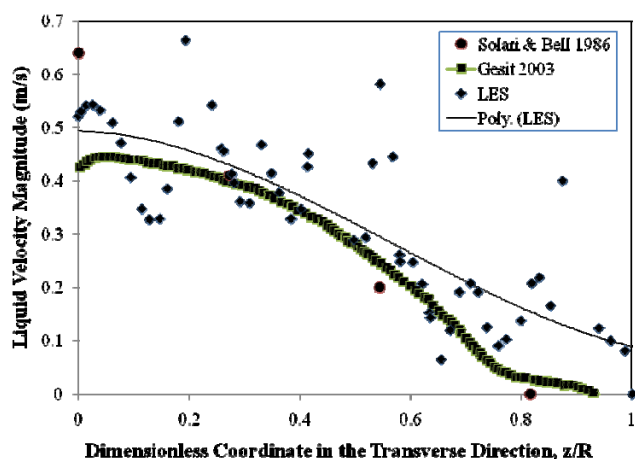


**Fig. 8.** Downstream liquid velocity profile at  $Q_L=17.8 \times 10^{-3} \text{ m}^3/\text{s}$  and  $F_S = 0.462$ .

## VII. CONCLUSION

The present work attempts to model the hydrodynamics of industrial-scale sieve tray using VOF-LES model. The flow behavior in distillation tray was modeled as three dimensional two-phase flows of gas and liquid. The governing equations, (1)-(14), are solved using the FLUENT

code. Computational results are validated by means of comparison of quantities such as clear-liquid height and liquid velocity profiles with published experimental results [1] and available correlations [7], [8]. In overall, the computational results show very good agreement with experimental data.

Massive efforts and resources have been spent in the past decades to understand the complex flow behavior prevailing in the distillation sieve tray. However, till present, having so many published correlations, uncertainties still exist in the design of sieve tray. This work has, however, proven that CFD method is able to answer those uncertainties effectively. Clear liquid height was computed with remarkable accuracy and the prevailing flow regime was predicted very well for this given operating conditions. In conclusion, the proposed VOF-LES model has successfully modeled the hydrodynamics of distillation sieve tray and thus can be utilized with high confidence in the optimization of tray design.

## REFERENCES

- [1] Solari, R. B., and Bell, R. L., "Fluid Flow Patterns and velocity Distribution on Commercial-Scale Sieve Trays," *American Institute of Chemical Engineering Journal*, vol. 32, pp. 640-649, 1986.
- [2] Mehta, B., Chuang, K. T., and Nandakumar, K., "Model for liquid phase flow on sieve tray," *Chemical Engineering Research and Design*, vol. 76, pp. 843-848, 1998.
- [3] Yu, K. T., Yuan, X. G., You, X. Y., and Liu, C. J., "Computational fluid-dynamics and experimental verification of two-phase flow on a sieve column tray," *Chemical Engineering Research and Design*, vol. 77(a), pp. 712-717, 1999.
- [4] Porter, K. E., Yu, K. T., Chambers, S., and Zhang, M. Q., "Flow Patterns and Temperature Profiles on a 2.44 m Diameter Sieve Tray," *Transaction of Institute of Chemical Engineering*, vol. 70(a), pp. 489-500, 1992.
- [5] Krishna, R., van Baten, J. M., Ellenberger, J., Higler, A. P., and Taylor, R., "CFD Simulations of Sieve Tray Hydrodynamics," *Transaction of Institute of Chemical Engineering*, vol. 77(a), pp. 639-646, 1999.
- [6] Kister, H. Z., *Distillation Design*, New York: McGraw-Hill, 1992, pp. 318.
- [7] Bennett, D. L., Agrawal, R., and Cook, P. J., "New Pressure Drop Correlation for Sieve Tray Distillation Columns," *American Institute of Chemical Engineering Journal*, vol. 29, pp. 434-442, 1983.
- [8] Colwell, C. J., "Clear Liquid Height and Froth Density on Sieve Trays," *American Institute of Chemical Engineering Journal*, vol. 20, pp. 298-307, 1981.
- [9] van Baten, J. M., and Krishna, R., "Modeling sieve tray hydraulics using computational fluid dynamics," *Chemical Engineering Journal*, vol. 77, pp. 143-151, 2000.
- [10] Gesit, G., Nandakumar, K., and Chuang, K. T., "CFD Modeling of patterns and hydraulics of commercial-scale sieve trays," *American Institute of Chemical Engineering Journal*, vol. 49, pp. 910-924.
- [11] Bradshaw, P., Launder, B. E., and Lumley, J. L., "Collaborative Testing of Turbulence Models (Data Bank Contribution)," *Journal of Fluid Engineering*, vol. 118, pp. 143-247, 1996.
- [12] Brackbill, J. U., Kothe, D. B., and Zemach, C., "A continuum method for modeling surface tension," *Journal of Computational Physics*, vol. 100, pp. 335-354, 1992.
- [13] Smagorinsky, J., "General Circulation Experiments with the Primitive Equations, I. The Basic Experiment," *Monthly Weather Review*, vol. 19, pp. 99-164, March 1963.
- [14] Zienkiewicz, O. C., Taylor, R. L., and Nithiarasu, P., "The Finite Element Method for Fluid Dynamics, 6<sup>th</sup> Ed, Oxford: Elsevier Butterworth-Heinemann, 2005, pp. 269.
- [15] FLUENT Inc., "FLUENT 6.3. User's Manual," September 2006, pp. 23.21 - 23.25.